Available online at www.sciencedirect.com

SCIENCE DIRECT®

ELSEVIER

Palaeogeography, Palaeoclimatology, Palaeoecology 217 (2005) 205–222

PALAEO

www.elsevier.com/locate/palaeo

Middle to late Miocene oxygen isotope stratigraphy of ODP site 1085 (SE Atlantic): new constrains on Miocene climate variability and sea-level fluctuations

T. Westerhold*, T. Bickert, U. Röhl

Fachbereich Geowissenschaften, Universität Bremen, 28334 Bremen, Germany

Received 9 December 2003; received in revised form 11 October 2004; accepted 19 November 2004

Abstract

The middle Miocene $\delta^{18}O$ increase represents a fundamental change in earth's climate system due to a major expansion and permanent establishment of the East Antarctic Ice Sheet accompanied by some effect of deepwater cooling. The long-term cooling trend in the middle to late Miocene was superimposed by several punctuated periods of glaciations (Mi-Events) characterized by oxygen isotopic shifts that have been related to the waxing and waning of the Antarctic ice-sheet and bottom water cooling.

Here, we present a high-resolution benthic stable oxygen isotope record from ODP Site 1085 located at the southwestern African continental margin that provides a detailed chronology for the middle to late Miocene (13.9–7.3 Ma) climate transition in the eastern South Atlantic. A composite Fe intensity record obtained by XRF core scanning ODP Sites 1085 and 1087 was used to construct an astronomically calibrated chronology based on orbital tuning. The oxygen isotope data exhibit four distinct $\delta^{18}O$ excursions, which have astronomical ages of 13.8, 13.2, 11.7, and 10.4 Ma and correspond to the Mi3, Mi4, Mi5, and Mi6 events. A global climate record was extracted from the oxygen isotopic composition. Both long- and short-term variabilities in the climate record are discussed in terms of sea-level and deep-water temperature changes. The oxygen isotope data support a causal link between sequence boundaries traced from the shelf and glacioeustatic changes due to ice-sheet growth.

Spectral analysis of the benthic $\delta^{18}O$ record shows strong power in the 400-kyr and 100-kyr bands documenting a paleoceanographic response to eccentricity-modulated variations in precession. A spectral peak around 180-kyr might be related to the asymmetry of the obliquity cycle indicating that the response of the dominantly unipolar Antarctic ice-sheet to obliquity-induced variations probably controlled the middle to late Miocene climate system. Maxima in the $\delta^{18}O$ record, interpreted as glacial periods, correspond to minima in 100-kyr eccentricity cycle and minima in the 174-kyr obliquity modulation. Strong middle to late Miocene glacial events are associated with 400-kyr eccentricity minima and obliquity modulation minima. Thus, fluctuations in the amplitude of obliquity and eccentricity seem to be the driving force for the middle to late Miocene climate variability.

Keywords: ODP Site 1085; Miocene; Oxygen isotopes; Astrochronology; Mi events; Sea-level

* Corresponding author. Tel.: +49 421 2188913; fax: +49 421 2188916.
E-mail address: tho@uni-bremen.de (T. Westerhold).

0031-0182/$ - see front matter © 2004 Elsevier B.V. All rights reserved.
doi:10.1016/j.palaeo.2004.12.001

1. Introduction

The Neogene period comprises a major change in climate state from relatively global warmth of the early Miocene to colder climates at the end of the Pliocene. As inferred from co-varying $\delta^{18}O$ values of planktonic and benthic foraminifers, the general cooling trend in the middle to late Miocene was superimposed by several punctuated periods of intensive glaciations (Mi-Events) which supposedly reflect continental ice sheet growth and/or bottom water cooling (Miller et al., 1991; Lear et al., 2000; Turco et al., 2001; Billups and Schrag, 2002). Due to the scarcity of continuous marine records spanning the middle to late Miocene, a period of widespread erosion in the deep sea (Keller and Barron, 1987), the characteristics of and the control on the Miocene glacial events is controversial. Recently, astronomically calibrated ages for the Mi5 and Mi6 event showed (Turco et al., 2001) that these coincide with periods of low-amplitude variations in obliquity related to the ~1.2 Ma cycle as proposed by Lourens and Hilgen (1997).

ODP Site 1085 is one of the most expanded and complete middle to late Miocene marine records retrieved from the Southwest African continental margin during ODP Leg 175. In this paper we present a unique high-resolution benthic oxygen isotope record spanning the middle to late Miocene (13.8–7.3 Ma). In addition, an astronomically calibrated time scale based on tuning of a composite Iron (Fe) intensity record from ODP Sites 1085 and 1087 has been constructed. For the first time, this high-resolution $\delta^{18}O$ record enables us to decipher the driving mechanisms of the middle to late Miocene climate system in detail. Therefore, this study focuses on the characterization and timing of the Mi-events, the orbital control of $\delta^{18}O$ variability, and inferences on sea-level fluctuation during the middle to late Miocene.

2. Material and methods

ODP Holes 1085A and 1087C were drilled in the Cape Basin during Leg 175. ODP Site 1085 is located at the southwestern African continental margin (Fig. 1) (29°22.47′ S, 13°59.41′ E, 1713 m water depth) off the mouth of the Orange River, a perennial river discharging into the South Atlantic (Wefer et al., 1998). A continuous hemipelagic sedimentary section composed of nannofossils ooze, diluted by various amounts silt and clay, was recovered from Site 1085 reaching down to the middle Miocene (14 Ma). The studied interval (350–600 mbsf) spanning the Middle to the Late Miocene has no composite section, but shows a mean recovery of over 100% with an average sedimentation rate of 3–5 cm/kyr (Wefer et al., 1998). Today, Site 1085 is bathed primarily in the Upper Circumpolar Deep Water (UCDW) near the mixing zone with the North Atlantic Deep Water (NADW) (Wefer et al., 1998). ODP Site 1087 is located further south at the continental margin (31°27.91′ S, 15°18.65′ E, 1372 m water depth). Sediments recovered from Site 1087 down to 430 mbsf span the last 10 Ma with sedimentation rates ranging from 2 to 7 cm/kyr and represent a relatively continuous pelagic section, rich in carbonate and poor in organic carbon (Wefer et al., 1998). The lowermost 70 m contain middle Miocene to early Oligocene sediment layers interrupted by at least two major discontinuities.

Continuous measurements of the elemental composition of sediments at ODP Sites 1085A and 1087C were performed at the Bremen ODP Core Repository (BCR) using the X-ray fluorescence (XRF) core scanner (Röhl and Abrams, 2000), which allows high-resolution, nearly continuous, non-destructive analyses of major and minor elements at the surface of split cores (Jansen et al., 1998). The XRF core scanner at the BCR is equipped with a molybdenum X-ray source (3–50 kV), a Peltier-cooled PSI detector (Kevex™) with a 125-μm beryllium window and a multi channel analyzer with a 20-eV spectral resolution. This system configuration allows the analysis of elements from potassium (K, atomic number 19) through strontium (Sr, atomic number 38; at 20 kV X-ray voltage). XRF data were collected every 4 cm downcore over a 1 cm^2 area using 30-s count time and an X-ray current of 0.087 mA to obtain the elemental concentration of Fe. More than 240 m of core from Site 1085A (42X through 63X, 382–594 mbsf) were analyzed. The data from 353.4 to 392.45 mbsf (39X through 41X) are taken from Vidal et al. (2002). The entire record represents the time period from about 6.5 to 13.9 Ma. From Site 1087C, approximately 144 m (30X through 44X, 261–405 mbsf) were scanned,

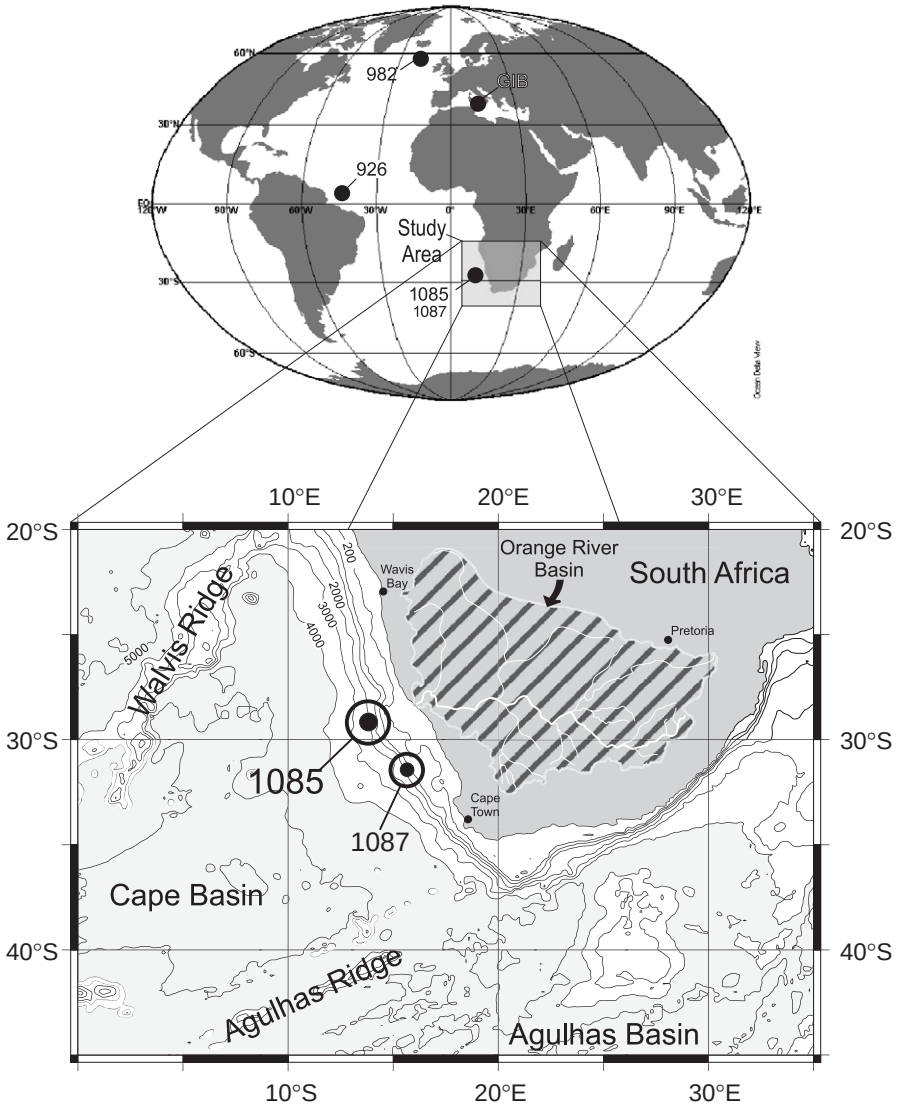

Fig. 1. Location map showing the positions of ODP-Sites 1085 and 1087 off Southwest Africa. The Orange River and the inflow of minor rivers are displayed. The catchment area of the Orange River in South Africa is hatched (Orange River Basin). Ocean areas deeper than 4000 m are shaded in light gray. The global map shows the position of ODP Sites 982, 926, 1085, and the location of the Monte Gibliscemi record (GIB).

corresponding to the time from 6.5 to 10.2 Ma. Based upon the biostratigraphic age model, the step size of 4 cm represents a temporal resolution of 1000 to 2500 years.

Benthic stable oxygen isotope data were generated from analysis of the epifaunal benthic foraminifera *Cibicidoides wuellerstorfi* or *Cibicidoides kullenbergi*. Isotope measurements were performed on a Finnigan MAT 252 mass spectrometer equipped with an automated carbonate preparation line at the University Bremen. The carbonate was reacted with orthophosphoric acid at 75 °C. Analytical precision is 0.07‰ for $\delta^{18}O$ as referred to an internal carbonate standard. All data are reported against the VPDB standard after calibration with NIST 19. The middle to late Miocene section was sampled every 10 cm along

the shipboard mbsf (Cores 1085A—42X through 63X). The total number of samples analyzed was 2622. A number of 714 duplicate analyses of *C. kullenbergi* and *C. wuellerstorfi* prove that no correction between both species is necessary in the middle to late Miocene section (Fig. 5b).

All data and tables are available at PANGAEA—Network for Geological and Environmental Data (www.pangaea.de).

3. Results and chronostratigraphy

3.1. XRF data

In Fig. 2, Fe intensities derived from the XRF core logs of hole 1085A and 1087C, respectively, are plotted versus log-depth (mbsf; Tables 1 and 2). Fe intensities vary between 500 and 6000 cps, and show high-frequency cyclicity. The long-term trend in the Fe intensity data is characterized by six periods of higher Fe intensity located at 433–453, 470–481, 528–537, 547–553, 556–561, and 565–570 m log-depth. These periods correspond to the middle to late Miocene carbonate crash events in the Southeast Atlantic (Westerhold, 2003). At hole 1087C, Fe intensities vary between 500 and 2500 cps. The XRF intensity record of Site 1087 reaches down to 405 mbsf, below which a hiatus is located. Two periods from 433 to 453 and from 470 to 475 m log-depth reveal enhanced Fe intensities. For both Sites, the Fe records are used as proxies for terrigenous sedimentation.

3.2. Composite section

At Sites 1085 and 1087, a composite depth scale was established only for the upper 300 and 200 m, respectively, based on splicing together the susceptibility records of multiple holes at these sites (Wefer et al., 1998). Below, single hole drilling prevented continuous splicing. Due to the similarity of the Fe-records, we established a composite record by correlating holes 1085A and 1087C. Using Fe-intensities of the XRF measurements as the primary hole-to-hole correlation tool, each core at Sites 1085A and 1087C was then individually correlated to the corresponding downhole logging interval of the Total Gamma Ray (SGR) measurements gained by the Natural Gamma Tool (NGT) string in Hole 1085A (Fig. 2). This procedure provides the opportunity to create a spliced Fe record of 1085A unaffected by drilling disturbances (e.g., Hagelberg et al., 1992). The NGT measures the spectrum of natural gamma ray radiation of a formation resolving the spectrum into the three most common compounds of the naturally occurring radiation: potassium, thorium, and uranium. Potassium and thorium are the primary radioactive elements present in clays, whereas thorium is frequently found in ash layers. Therefore, it is assumed that higher amounts of terrestrial material in the sediment will be reflected by higher SGR values, and thus consequently correlate with high intensities in the Fe record of Sites 1085A and 1087C. Regardless of the absolute depth value, relative thickness and spacing of features displayed on SGR and other downhole measurements should be identical within the limits of varying vertical resolution capabilities. Fig. 2 shows the correlation with reference to the SGR logging depth of Site 1085A, which is referred to as the meters log-depth hereafter. The tie points to create the new composite depth for the Fe intensity record of Site 1085A and 1087C based on the SGR logging depth of the NGT tool are listed in Tables 3 and 4. Completing the correlation, gaps between each core in Site 1085A were filled with the appropriate Fe intensity data from Site 1087C to create a composite Fe intensity record for Site 1085. The tie points are given in Table 5. Due to the lower Fe concentration in 1087C the intensity data have been adjusted to the intensity level of 1085A by multiplying an arbitrary factor taking care not to alter the original variation signal. The spliced Fe intensity data were then used for orbital tuning without smoothing or stacking of data.

The complete composite record for Site 1085 has been created from 353.60 down to 460.83 m log-depth. Due to the slump deposition in Site 1087C below 409 mbsf, the composite record for Site 1085 was extended from 460.85 down to 555.04 m log-depth by correlation to the SGR log revealing the size of core-break gaps. The maximum extent of core-brake gaps in this interval was 0.7 m which corresponds to less than a obliquity cycle according to biostratigraphy. From 555.82 down to 593.57 m log-depth, correlation to the SGR log was impossible. Therefore cores had to be adjusted, considering that mcd values exceed mbsf

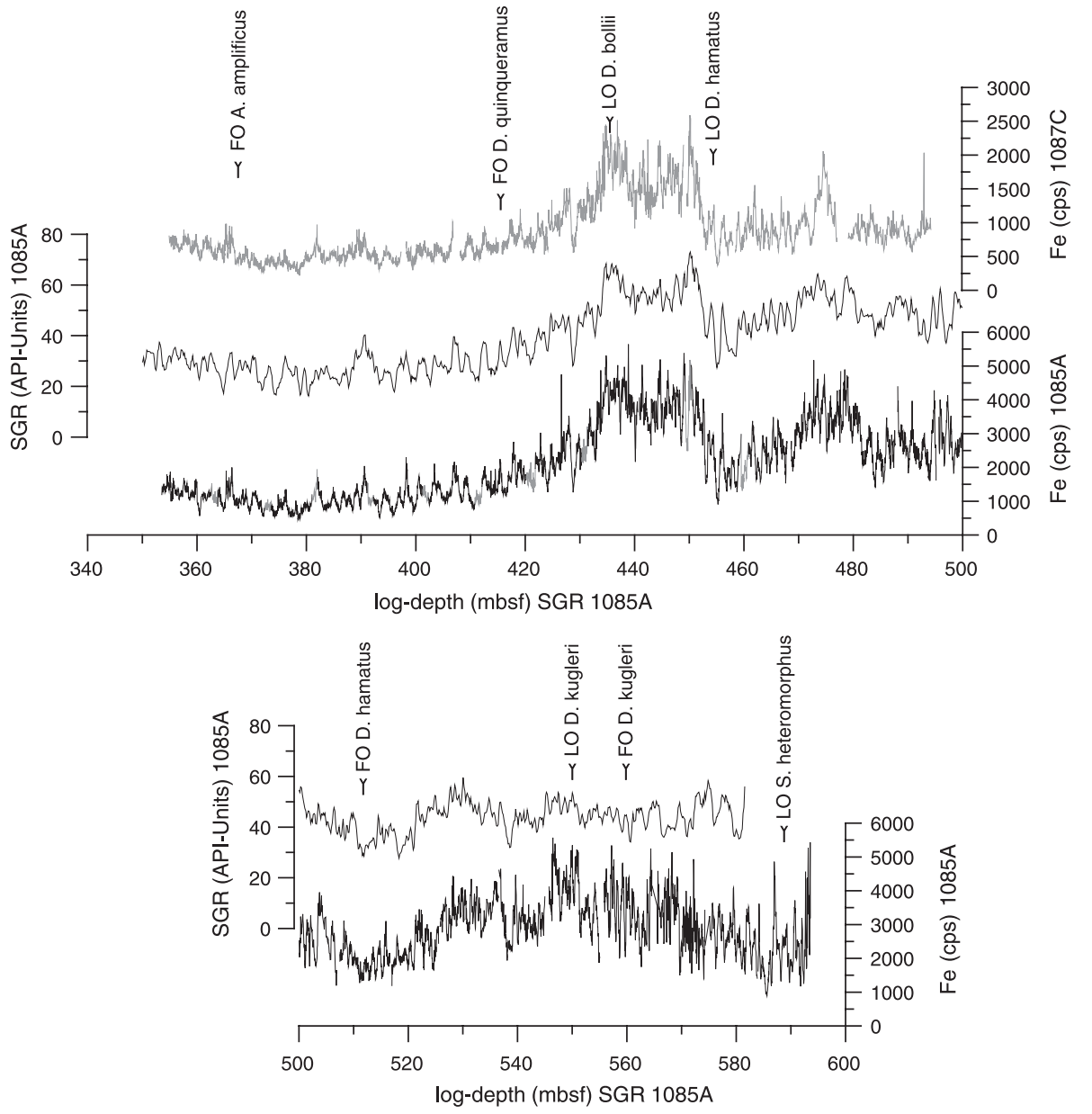

Fig. 2. Composite section for hole 1085A and 1087C. The Fe intensities are plotted for holes 1085A and 1087C. These two logs are correlated to the SGR-log depth of the Gamma Ray Spectrometry-Dual Induction Tool String (NGT-DIT) of hole 1085A. For the creation of a composite Fe-intensity record, the gaps in 1085A are filled with data from the Fe-log of 1087C. Below 555 mcd, the record of 1085A cannot be tuned to the SGR-log. For discussion, see text. Arrows indicate the position of the shipboard nannofossils biostratigraphy (Wefer et al., 1998).

values by about 10% at Site 1085A as observed by Wefer et al. (1998). To account for this expansion, each core in this part of the record was compressed by 10%. Core gaps in this interval have a maximum extent of 0.8 m corresponding to less than half of an eccentricity cycle according to the biostratigraphy.

3.3. Orbital tuning

Shipboard data of the biostratigraphic datums and the paleomagnetic events provided the preliminary age model for Site 1085 (Wefer et al., 1998). Because of coring-induced magnetization (CIM), the magnetostratigraphic interpretation at Site 1085A was only possible down to the bottom of Chron C3n.4n at 5.23 Ma at 280 mbsf (Wefer et al., 1998) precluding a magnetostratigraphic-supported age model for the middle to late Miocene. Thus, the stratigraphic framework needed for orbital tuning is based on the biostratigraphy established during Leg 175 using the integrated time scale of Berggren et al. (1995a,b). We chose calcareous nannofossil datums only, because they have been shown to give more reliable datums than those derived from foraminifera (e.g., Backman and Raffi, 1997). The biostratigraphic ages are based on core-catcher samples and thus a maximum error of 9.6 m or 200 kyr was taken into consideration.

As shown by Christensen and Maslin (2001), and Vidal et al. (2002) eccentricity modulates the signals derived from terrigenous material (magnetic susceptibility, XRF Fe record) in the Cape Basin. Maxima in eccentricity correspond to maxima in the terrigenous signal (Vidal et al., 2002). Therefore, we first examined the cyclic fluctuations of the Fe intensity record by using the preliminary age model from biostratigraphy with the help of the AnalySeries software package (Paillard et al., 1996). Frequency spectra of the Fe record revealed that much of the spectral power is concentrated in the low-frequency domain (Fig. 3). Peaks are observed close to 400 kyr and 100 kyr. Comparing the biostratigraphically dated Fe record to the target curve, 400 kyr and 100 kyr peaks are apparent, although the power spectrum is shifted relative to that of the ETP target. The absence of distinct variance related to precession is related to the origin of the terrigenous fraction at Site 1085 (Vidal et al., 2002). Comparison between the Fe and $\delta^{18}O$ records shows that Fe content is higher in interglacial periods pointing to enhanced river runoff in interglacial like conditions, similar to the late Miocene and early Pliocene sedimentation pattern at Site 1085 (Vidal et al., 2002). This implies that high Fe intensities are associated with eccentricity and/or obliquity maxima. Therefore, an astronomically calibrated age model for the Miocene section of ODP Site

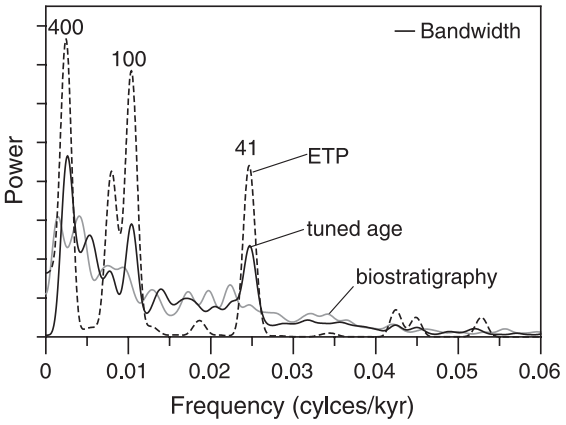

Fig. 3. Blackman–Tukey power spectrum of the ETP target curve, biostratigraphic age model, and the tuned composite Fe intensity age model computed with the AnalySeries software package (Paillard et al., 1996). Prior to spectral analysis, Fe intensity data have been high pass filtered at 0.002 Hz to remove variations above 500 kyr, low pass filtered at 0.075 Hz to remove noise below the 10-kyr period, normalized to unite variance and padded with zeros. Spectral estimates are based on a Parzen smoothing window with 410 lags and an interpolated time interval of 2 kyr.

1085 and 1087 was constructed by tuning the composite XRF-Fe intensity record to an Eccentricity–Tilt–Precession (ETP) target curve. We assumed no lag between the tuning target and the lithologic signal. In the absence of an identified mechanism for generating a lag during the Miocene in the region we are dealing with, we consider that our record has responded without delay. The ETP curve was generated by normalizing Eccentricity, Obliquity (Tilt), and Precession values (Laskar et al., 2004) and then combining it by the following expression: $E+0.5*T-0.5P$. Tuning was done by correlating prominent features of the Fe record to the ETP target curve. The record first was tuned in the 400-kyr domain (0.0025 ± 0.0005 cycles/kyr) and then in the 100-kyr domain (0.01 ± 0.003 cycles/kyr). In the tuning procedure, we followed a minimal tuning approach using as few tie-points as possible to avoid over-tuning. Because the recovery gaps in the lower part of Site 1085, where no composite section could be constructed, have a maximum extend of half of an eccentricity cycle, the determination of the eccentricity related component for orbital tuning will not be affected.

The age model derived from orbital tuning is presented in Table 6. A comparison of the individual

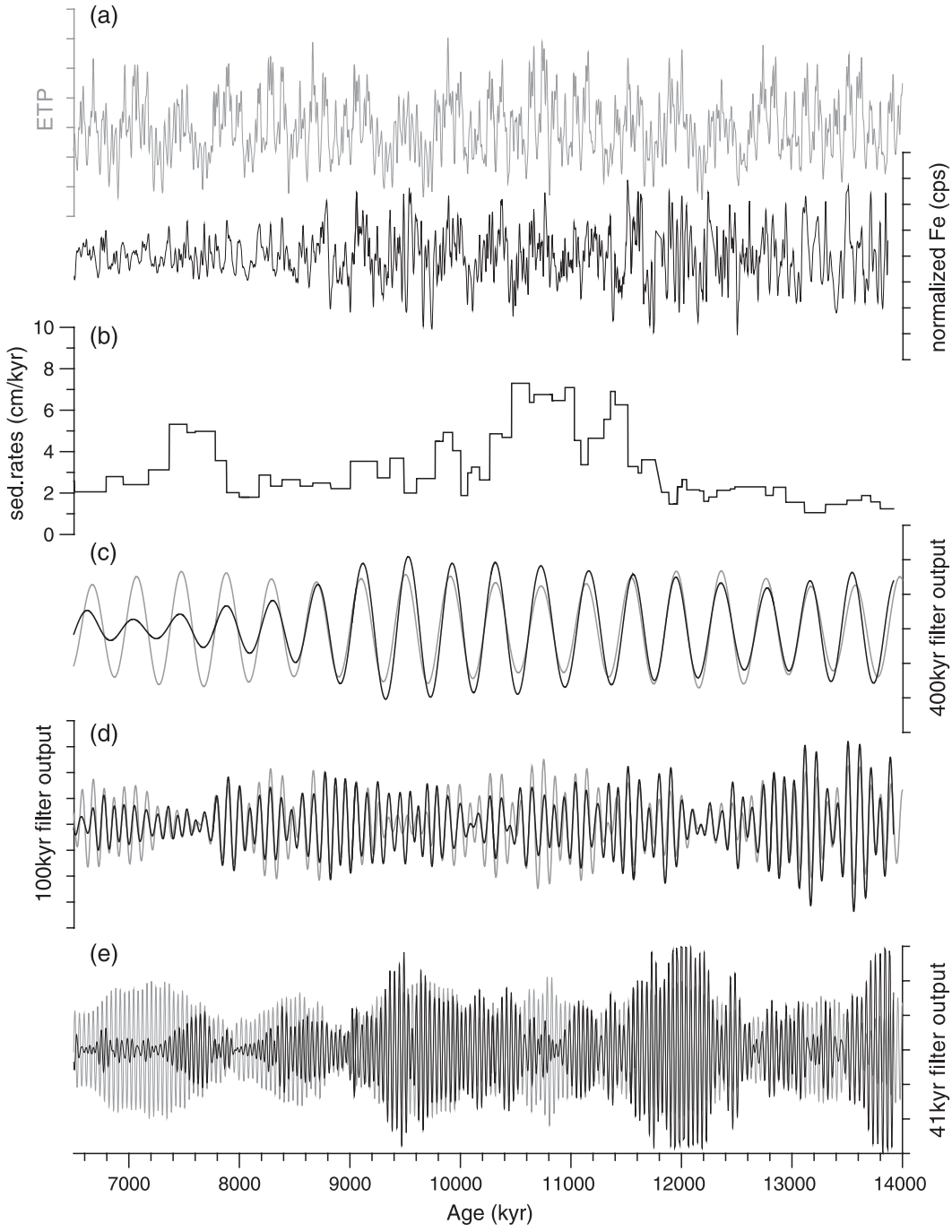

Fig. 4. Summary of the tuning results of Site 1085 composite Fe intensity. Panel a shows the normalized ETP target curve and the composite Fe intensity signal (smoothed by a 5-point weighted average, high-pass filtered at 500 kyr, normalized) plotted vs. age. In panel b, the sedimentation rates based on the orbital tuning are plotted. Panels c, d, and e show a comparison of the filtered time series (solid black line represents the Fe intensity, solid grey line represents the ETP target) at the 400-kyr, the 100-kyr, and the 41-kyr bands, respectively. For comparison, all data have been normalized to unite variance.

400-kyr (Fig. 4c) and 100-kyr cycles (Fig. 4d) yield a good match throughout the record. The normalized Fe intensity record (Fig. 4a) reveals distinct 400-kyr cycles with low Fe intensity regions corresponding to the 400 kyr minima in eccentricity from 6.5 to 14 Ma. The 100-kyr filter output of the Fe data shows the 400-kyr amplitude modulation of the eccentricity signal supporting the tuning strategy. A closer look at the Fe data and the ETP target curve shows remarkable similarities down to precessional scale (Fig. 4a). Due to the excellent match of Fe data and ETP curve, we are confident that the accuracy of the tuned time scale is less than an obliquity cycle. We refrain from tuning the oxygen isotope record to obliquity because we want to investigate variations in the isotopic signal independent from direct tuning. During times of low amplitudes in the 100-kyr filter, the Fe record shows high amplitudes in the obliquity component (Fig. 4e). After 9 Ma, the overall amplitude in the filtered outputs decrease and the obliquity component appears to be of minor importance in the Fe record. The tuned orbital time scale for the part from 7.3 to 6.5 Ma is consistent with the results of Vidal et al. (2002). Because our $\delta^{18}O$ record starts at 7.3 Ma, the discussion will focus on the period from 7.3 to 13.9 Ma hereafter. The derived sedimentation rates (Fig. 4b) range between 1 and 7.3 cm/kyr. From 14 up to 11.7 Ma, the sedimentation rates are well below 4 cm/kyr. Then they steadily increase to 7 cm/kyr remaining at that value from 11.5 to 10.4 Ma, punctuated by a drop in sedimentation rates at 11.1 Ma. Thereafter, rates decrease to an average value of 3 cm/kyr till 6.5 Ma, interrupted by enhanced sedimentation rates at 9.9 Ma and around 7.6 Ma.

3.4. Oxygen isotope data

Oxygen isotope data (Table 7) from the middle to late Miocene section of Site 1085 are presented as raw data vs. age in Fig. 5. In the investigated period, the $\delta^{18}O$ values increase from 1.5‰ to 2.4‰ and show an average variation in amplitude by 0.4‰. The long-

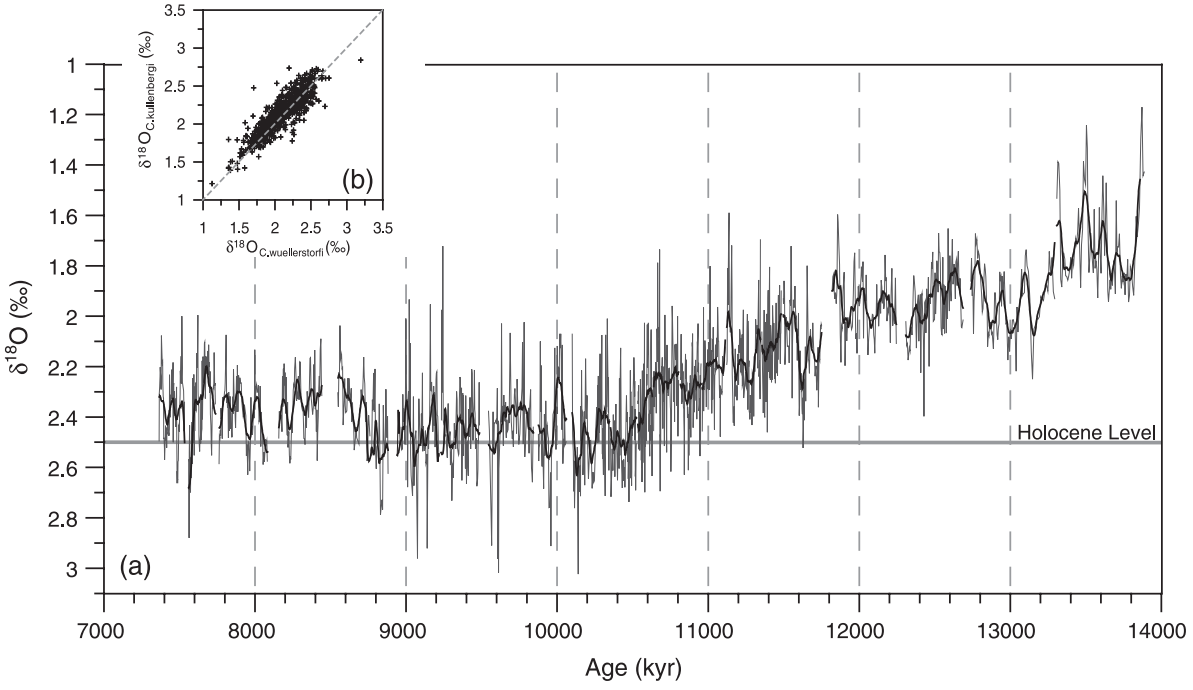

Fig. 5. (a) Benthic foraminiferal $\delta^{18}O$ data from Site 1085A versus age. Holocene stable oxygen isotope mean value (horizontal black line) for Site 1085 is from Westerhold et al. (submitted for publication). Black solid curve represents a 51-kyr moving average. $\delta^{18}O$ values are not adjusted for isotopic disequilibrium. (b) Oxygen isotope measurements of specimens of *Cibicidoides wuellerstorfi* and *Cibicidoides kullenbergi* from the same sample (n=714). Note that the trend follows a 1:1 relationship for $\delta^{18}O$.

term increase from 13.8 to 10.4 Ma follows the general trend in benthic stable isotopes throughout the Neogene as compiled by Zachos et al. (2001a) from 40 DSDP and ODP Legs. This development reflects the middle Miocene buildup of the East Antarctic Ice Sheet between 15 and 11 Ma. At Site 1085 the $\delta^{18}O$ values reach Holocene levels at the end of the long-term cooling trend at 10.4 Ma. Superimposed on this long-term trend are punctuated episodes with clearly increased values at 13.8, 13.2, 11.7, and 10.4 Ma with amplitudes of 0.4–0.7‰ (Fig. 5). These correspond to the Miocene Glacial Events (Mi-Events; Miller et al., 1991). After the long term increase a period (10.4–8.7 Ma) of relatively heavy $\delta^{18}O$ values around 2.4‰ with an amplitude of up to 0.6‰ follows. This period ends with a decrease in average $\delta^{18}O$ values of 0.3‰ at 8.7 Ma. From 8.7 to 7.3 Ma, $\delta^{18}O$ values reveal low frequency cyclicity (~100 kyr). In general, the amplitude of the Miocene $\delta^{18}O$ variations are smaller compared to the Pleistocene benthic glacial–interglacial change of up to 1.5‰ documented at Site 1085 (Westerhold et al., submitted for publication).

4. Discussion

4.1. Miocene isotopic events

The middle to late Miocene open-ocean $\delta^{18}O$ record in the investigated time period is punctuated by five episodes of increased values known as the Mi3 through Mi7 events (Miller and Feigenson, 1991; Miller et al., 1991; Wright and Miller, 1992; Wright et al., 1992). These oxygen isotopic shifts have been ascribed to a combination of glacioeustatic sea-level lowering and bottom water cooling of 1–2 °C, but are primarily related to the waxing and waning of the Antarctic ice-sheet (Miller et al., 1991).

The Mi3 and Mi4 events constitute the two-step middle Miocene $\delta^{18}O$ increase (Savin et al., 1975; Shackleton and Kennett, 1975) with increases of between 0.5‰ and 0.8‰ (Miller et al., 1991). The Mi3 event was found within chron C5ABr by Miller et al. (1991) at about 13.6 Ma and the Mi4 event was found across the C5AAn/C5An transition (Miller et al., 1991) with peak values at the base of chron C5Ar at ~13 Ma, GPTS ages are after Cande and Kent (1995). The $\delta^{18}O$ record of Site 1085 shows an increase in $\delta^{18}O$ of 0.3‰ at the end of the investigated record (Fig. 6) interpreted as the Mi3 event. Furthermore, around 13.2 Ma, $\delta^{18}O$ values increase by 0.5‰ resembling the Mi4 event which showed a similar increase in benthic $\delta^{18}O$ values at DSDP Sites 563 and 608 (Miller et al., 1991). In our record, the Mi4 event appears first with a 0.5‰ increase in $\delta^{18}O$ values within 200 kyr, followed by two saw-tooth like $\delta^{18}O$ variations with a duration of 120 kyr each. Mi4 ends with an increase in $\delta^{18}O$ values of 0.3‰ at 12.8 Ma. The timing of the Mi4 event centered at 13.0 Ma in Site 1085 shows an age discrepancy of 200 kyr with a previously predicted age of 12.8 Ma (Lourens and Hilgen, 1997). But the $\delta^{18}O$ record of ODP Site 926 from the western Equatorial Atlantic (Shackleton and Hall, 1997) with an orbitally tuned timescale (Shackleton and Crowhurst, 1997) reveals an increase by 0.5‰ around 13.2 Ma, supporting our age estimate of the onset of Mi4. Additionally, the $\delta^{18}O$ record at Site 926 shows decreasing values around 12.7 Ma corresponding to the proposed age of the Mi4 event at Site 1085. If we now compare the isotope records to the global composite of Zachos et al. (2001a), the Mi3 event can and the Mi4 event cannot be clearly recognized. Looking at the $\delta^{18}O$ record of Site 1085 one might argue that the minimum at ~13.5 Ma might correlate with the 13.25 Ma $\delta^{18}O$ minimum in the global record. This suggests that the $\delta^{18}O$ record of Site 1085 would be too old by up to 250 kyr. Comparison of unpublished $\delta^{13}C$ data from Site 1085 with the $\delta^{13}C$ record of Site 761B (Holbourn et al., 2004) confirms our tuning. The reason for the discrepancy to the global compilation is the rather low resolution of the compilation in the middle to late Miocene as well as the combination of data from all over the world oceans having rather large uncertainties in their age models. This is clearly seen in the vicinity of the Mi4 event (~13 Ma), which has no expression in the global compilation but can be traced in the 926 record. Rather small discrepancies between the Ceara Rise record and Site 1085 are probably due to uncertainties in the tuning of both records (Site 1085 is not tuned to obliquity) and the lower resolution of the $\delta^{18}O$ record of the Ceara Rise because of aliasing. The onset of the Mi4 event, which we place at ~13.2 Ma, might be slightly too old in the Site 1085 record because the core break might have been longer than predicted.

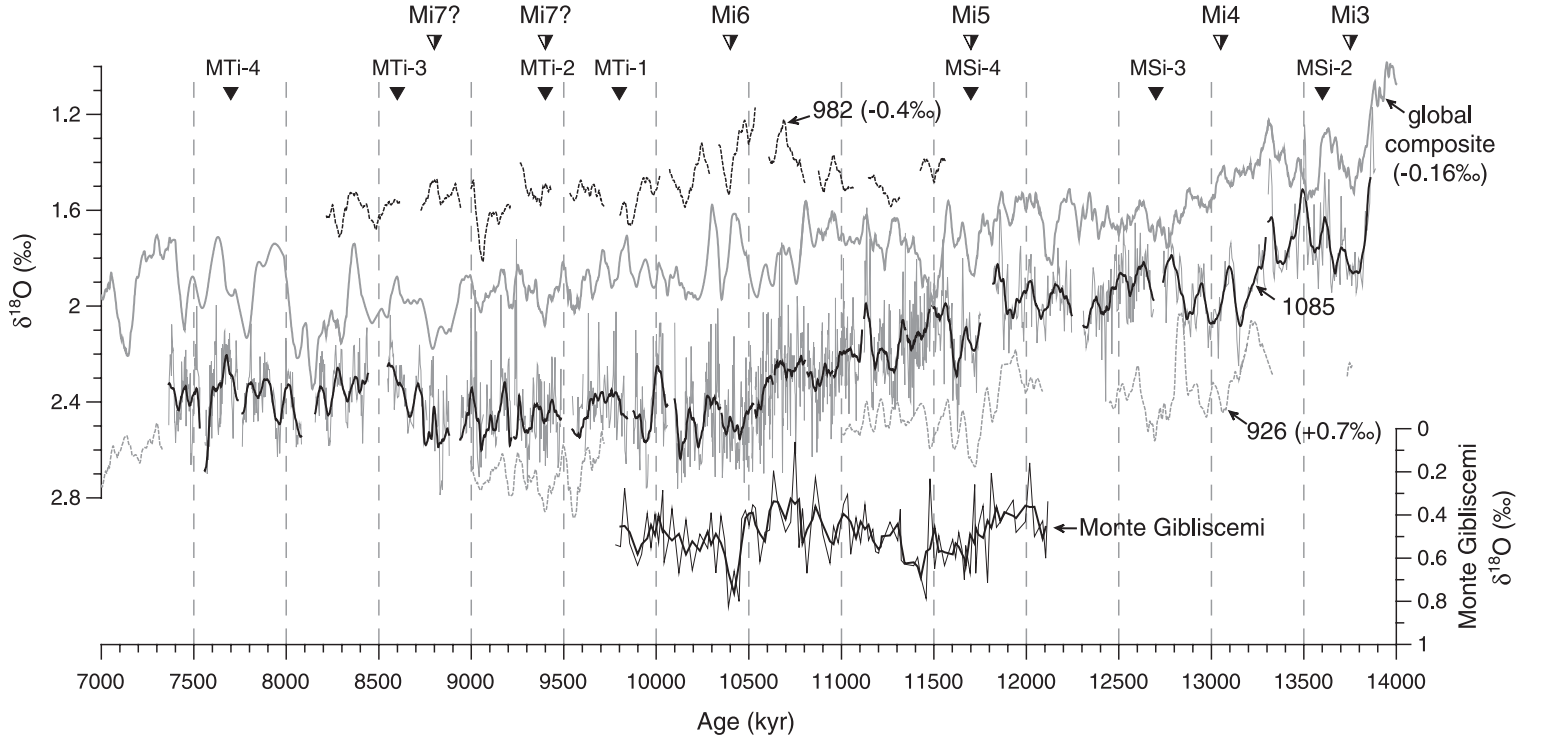

Fig. 6. Comparison between the long-term trends in the benthic stable oxygen isotope record from ODP Site 1085 (solid black line is the 50-kyr moving average, light grey line are the raw data), ODP Site 926 (dashed gray line; Shackleton and Hall, 1997), ODP Site 982 (dashed black line; Andersson and Jansen, 2003), the global deep sea composite of Zachos et al. (2001a) (solid grey line), and the Monte Gibliscemi record (thin black line with 51-kyr moving average represented by the solid gray line; Turco et al., 2001). All $\delta^{18}O$ records have been smoothed using a 50-kyr moving average and are not adjusted for isotopic disequilibrium. To separate the $\delta^{18}O$ data of ODP Site 926 from the global deep-sea composite, which contains these data, we shifted the data of Site 926 by +0.7‰. The global composite is offset by −0.16‰ and the Site 982 record by −0.4‰ for comparison. The half-filled triangles indicate the ages for Mi3, Mi4, Mi5, Mi6, and Mi7 as suggested in this study. The filled triangles indicate the ages and names of the oxygen isotope events defined by Abreu and Anderson (1998).

The Mi5 event is positioned at the base of chron C5r by Miller et al. (1991) at about 11.7 Ma and biostratigraphically within the range of *D. kugleri* (Turco et al., 2001) between 11.868 and 11.573 Ma (ages after Turco et al., 2002). At Site 1085, the *D. kugleri* zone is located within a twofold $\delta^{18}O$ increase of overall 0.5‰ between 11.9 and 11.5 Ma, indicating that this increase corresponds to the Mi5 event (Fig. 4). Recent results from an astronomically dated deep marine succession in the Mediterranean indicate that the Mi5 event occurred at 11.4 (Turco et al., 2001), giving an age discrepancy with our estimate of almost 300 kyr. Shackleton and Hall (1997) proposed that a brief deep-water cooling event at 11.4 Ma might represent Mi5, but a much stronger shift in benthic $\delta^{18}O$ of about 0.4‰ occurs already between 11.8 and 11.7 Ma at Site 926. A closer look at the data of Turco et al. (2001) shows that the shift in $\delta^{18}O$ values already starts at 11.85 Ma reaching a maximum at 11.7 Ma. The proposed shift at 11.4 Ma is of lower amplitude and probably an artifact of smoothing. Comparing the $\delta^{18}O$ records, it seems that the Mi5 event consists of 3 to 4 maxima with an average duration of 100 kyr from 11.8 to 11.4 Ma.

The Mi6 event is found in the center of chron C5n at Site 608 (Miller and Feigenson, 1991) and recorded between the LO *C. miopelagicus* at 10.977 Ma (Hilgen et al., 2000) and the FO *D. hamatus* at 10.41 (age after Turco et al., 2002). In the $\delta^{18}O$ record of Site 1085, a major increase is documented from 10.7 to 10.4 Ma (Fig. 4). At 10.4 Ma, the heaviest $\delta^{18}O$ values are reached within the period from 13.8 to 10.2 Ma likely to resemble the Mi6 event. In the $\delta^{18}O$ record of Site 982 (Andersson and Jansen, 2003), Mi5 is poorly constrained because of a sampling gap, but Mi6 was identified between 10.55 and 10.4 Ma corresponding reasonably well with the increased $\delta^{18}O$ values at Site 1085 and the Mi6 event in the Gibliscemi record of Turco et al. (2001). After the shift of 0.3‰ at Site 1085, mean $\delta^{18}O$ values remain at an average of 2.5‰ from 10.4 to 8.7 Ma. Thereafter $\delta^{18}O$ values decrease by 0.2‰ towards an average of 2.3‰. Additional strong $\delta^{18}O$ maxima can also be found at 10.24 and 10.14 Ma reaching the highest values of the entire time span.

The Mi7 event is positioned in chron C4Ar.1n by Wright and Miller (1992) at 9.45 Ma. The $\delta^{18}O$ record of Site 1085 features no pronounced shift in the vicinity of the assigned age for Mi7 (Fig. 6). Amplitude variations of $\delta^{18}O$ values are in the order of 0.4‰ in this period. In western Equatorial Atlantic Site 926 (Shackleton and Hall, 1997) a pronounced maximum in $\delta^{18}O$ values occurs at 9.4 Ma, which corresponds to increased $\delta^{18}O$ values in Site 1085 as well. Generally, there is a good fit between $\delta^{18}O$ values of Site 926 and 1085 in the period from 9.7 to 9.0 Ma. Both records show numerous $\delta^{18}O$ events centered at 9.56, 9.40, 9.31, 9.22, 9.14, and 9.04, and therefore make it hard to identify one major event. The only marked increase in $\delta^{18}O$ at Northern Atlantic Site 982 (Andersson and Jansen, 2003) is located at 9.04 Ma suggesting that the Mi7 event might be located here. In contrast, comparison of $\delta^{18}O$ variations in the Northern Atlantic (Site 904) and sequence boundaries at the New Jersey margin suggested that the Mi7 event to be located around 8.7 Ma (Miller et al., 1998). At 8.8 Ma, $\delta^{18}O$ values show an increase at Site 1085 and the Zachos et al. (2001a) composite, which only consists of 4 data points from Site 360 in the interval from 8.9 to 8.7 Ma. Recapitulating, the position of the Mi7 event is rather uncertain. The global composite section (Zachos et al., 2001a) comprises low data coverage from 11 to 7 Ma hampering a direct comparison with the Site 1085 data. Moreover, most of the data in the interval from 8.5 to 7 Ma are from the Pacific which might explain the strong differences between 8.4 and 8.0 Ma.

As seen from the comparison of different $\delta^{18}O$ records (Fig. 6), identification of Mi-events during the middle to late Miocene transition is difficult because records in which Mi-events have first been recognized are low in resolution and lack an accurate time scale. Thus, undersampling a high-frequency $\delta^{18}O$ signal may alias the record and can yield spurious conclusions as shown by Pisias and Mix (1988). Aliasing can obscure the Mi-events making them difficult to recognize because amplitude variations are small (0.5–0.6‰) in the middle to late Miocene. This is also apparent when we compare the Mi-events with the positive oxygen isotope events (Fig. 6) defined by Abreu and Anderson (1998). Good agreement in terms of timing exists where amplitude shifts in the $\delta^{18}O$ records are in the order of 0.8–1.0‰. In this case, MSi-2 corresponds to Mi3 and MSi-4 to Mi5. In the late Miocene, there is less agreement in the assigned oxygen isotope events of Miller et al. (1991)

and Abreu and Anderson (1998) because the amplitude in $\delta^{18}O$ variations assigned as events is well below 0.5‰. The high-frequency variation in the $\delta^{18}O$ record of Site 1085 in late Miocene varies with an amplitude of about 0.5‰. As pointed out by Shackleton and Hall (1997) as well as Andersson and Jansen (2003) the $\delta^{18}O$ variability observed in late Miocene sediments is probably not appropriate as a correlation tool in the late Miocene. For further evaluation of the characteristics of the Mi-events and their potential for correlation of sedimentary sequences, additional high-resolution oxygen isotope records in the middle to late Miocene have to be compiled.

4.2. Orbital control of $\delta^{18}O$ variations in the middle to late Miocene

The Miocene climate system is dominated by orbitally induced oscillations (Zachos et al., 2001a; Paul et al., 2000; Shackleton et al., 1999; Zachos et al., 1997). The primary beat of the glaciated Cenozoic is the obliquity band, regardless of the state of other boundary conditions or the location of ice-sheets (Zachos et al., 2001a). It has been suggested that long-term astronomical variations in earth's orbit and inclination may have controlled the occurrence of the Mi-events (Beaufort, 1994; Lourens and Hilgen, 1997). Turco et al. (2001) ascribe the Mi5 and Mi6 events to periods of low-amplitude variations in obliquity, in contrast to the last 5.3 Ma when major steps in glacial ice buildup are related to increasing amplitude variations in obliquity (Lourens and Hilgen, 1997). Lourens and Hilgen (1997) argue that the average spacing between the Mi3 to Mi7 events closely matches the 1.2-Ma-long periodic variations in obliquity (Fig. 7), pointing to the sensitivity of ice-sheets to obliquity-generated changes in high-latitude insolation in the Miocene. The high-resolution $\delta^{18}O$ record of Site 1085 reveals that only the Mi3 and Mi6 event are associated with low-amplitude variations in obliquity. The Mi4 and Mi5 event are not associated with the 1.2 Ma obliquity minima (Fig. 7). Spectral analysis of the $\delta^{18}O$ record of Site 1085 reveals variable influence of different orbital frequencies (Fig. 8). The most interesting feature is a spectral peak around 180-kyr, which is close to the 174-kyr modulation of the obliquity cycle, ascribed to the asymmetry of the obliquity cycle (Liu, 1992), which has been recognized in several paleoclimatic records (e.g. Beaufort, 1994). Heavier $\delta^{18}O$ values in the Miocene Site 1085 record correspond to minima in the 174-kyr obliquity amplitude modulation (Fig. 7) suggesting that less warm summers favored ice growth as already proposed for the early Miocene (Zachos et al., 2001b). But the most important finding is that the numerous strong $\delta^{18}O$ maxima in the Site 1085 record are associated with minima in the 400-kyr eccentricity cycle (Fig. 7). The importance of the amplitude modulations of eccentricity for Miocene climate variability has been reported from the early Miocene (Zachos et al., 2001b). It has been proposed that extreme glaciations in the Miocene are induced by the coeval occurrence of prolonged eccentricity and obliquity minima (Zachos et al., 2001b). The Site 1085 $\delta^{18}O$ record suggests that glacial periods in the middle to late Miocene are induced by minima in eccentricity and minima in the 174-kyr obliquity modulation cycles (Fig. 7). The onset of the Mi3 event, for example, is located in a 400-kyr eccentricity minimum and a 174-kyr obliquity minimum, which is also close to a 1.2-Ma minimum in the obliquity modulation. But most interesting, nearly all $\delta^{18}O$ maxima in the Site 1085 record correspond to times of low obliquity and eccentricity (Fig. 7), except the Mi4 event. Thus, the combination of fluctuations in the amplitude of obliquity and eccentricity seems to be the driving force for the middle to late Miocene climate variability. The major difference between the Miocene and Pleistocene is the absence of large ice-sheets on the Northern Hemisphere and the open Central American Seaway in the Miocene (Zachos et al., 2001a). The fluctuations of the Northern Hemisphere ice-sheet are the driving force of the 100-kyr cycles during the Pleistocene (Imbrie et al., 1993). The Southern Hemisphere ice-sheets could have played a similar role with fluctuations large enough to induce 100-kyr cycles. The earliest evidence for ice-sheets on the Northern Hemisphere is the appearance of IRD at 12.6 Ma (Fronval and Jansen, 1996). Thus, an effect of both Northern and Southern Hemisphere polar ice-sheets can be expected, in which fluctuations of the larger Antarctic ice-sheets will have stronger implications on climate cycles. Clemens and Tiedemann (1997) also found eccentricity-related components in the $\delta^{18}O$ record of Site 659, which they related to an asymmetrical response

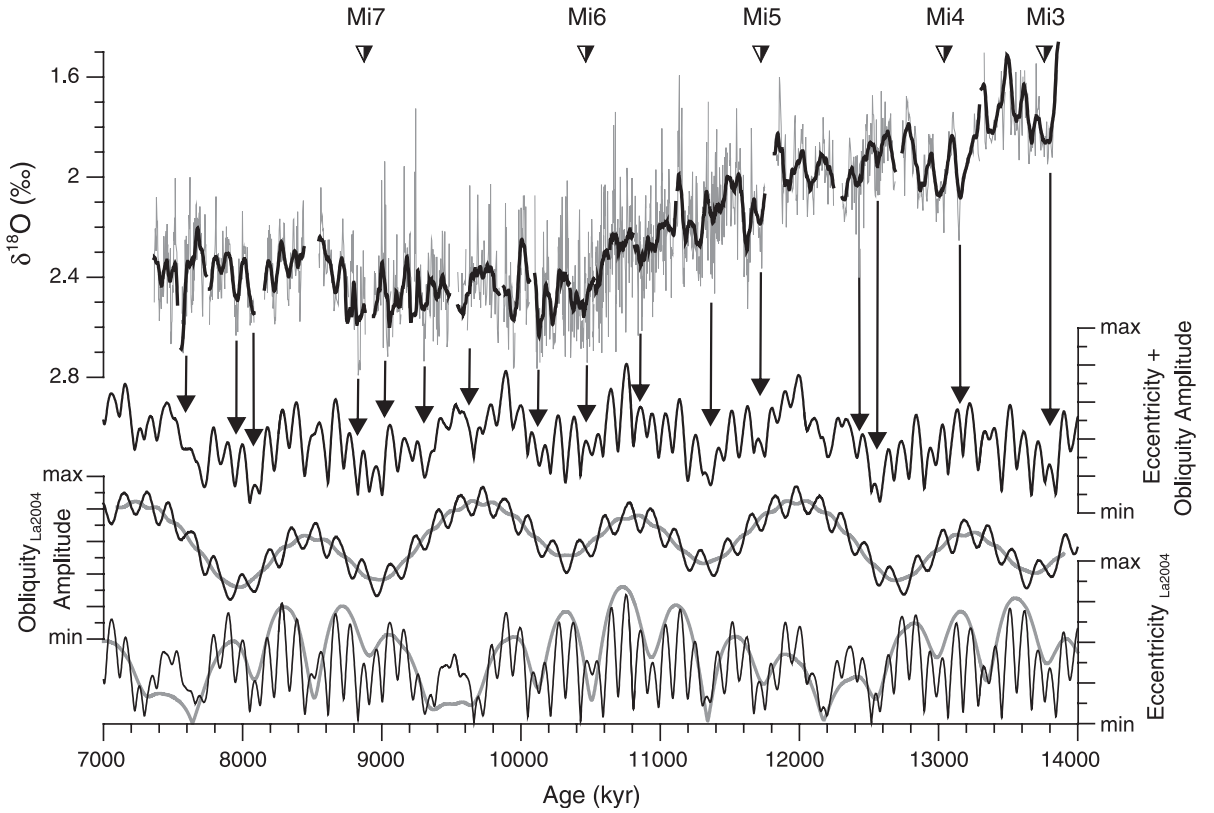

Fig. 7. Comparison between amplitude modulation of eccentricity and obliquity, and the Site 1085 $\delta^{18}O$ record. The lowermost panel shows orbital eccentricity (black line) and its 400-kyr modulation (grey line). Above that, the 174-kyr modulation of obliquity (dark grey line) and the 1.2 Ma minima in obliquity (light grey line) are plotted. The middle panel illustrates the combination of the 100-kyr eccentricity cycle and the 174-kyr obliquity amplitude modulation. Amplitude variations for eccentricity and obliquity (Laskar et al., 2004) in the 400-kyr band and in the 41-kyr band, respectively, have been calculated with the Program ENVELOPE (Schulz et al., 1999). The top panel shows the Site 1085 $\delta^{18}O$ data (raw data are light grey, 51-kyr moving average is bold solid line). Again, the proposed positions of the Mi-events are shown by half filled triangles. The arrows indicate the position of $\delta^{18}O$ maxima (glacial conditions) with respect to the combined eccentricity and obliquity amplitude modulation curve.

mechanism that preferentially introduces variance into the climate system from the warmer portion of the eccentricity-modulated precession cycle (Short et al., 1991).

4.3. Implications of site 1085 $\delta^{18}O$ record for the middle to late Miocene sea-level

The long-term trend in the $\delta^{18}O$ record exhibits a number of steps and peaks that reflect episodes of global warming and cooling, and ice-sheet growth and decay (Zachos et al., 2001a). The late middle Miocene climatic optimum (17–15 Ma) was followed by a gradual cooling and reestablishment of a major ice-sheet on Antarctica by 10 Ma (Vincent and Berger, 1985; Flower and Kennett, 1995; Zachos et al., 2001a). Lourens and Hilgen (1997) suggested a possible correlation between third-order eustatic cycles and glacial episodes (Mi-events) during the late Miocene. As documented by Miller et al. (1998), Miocene slope reflections at the New Jersey transect correlate with $\delta^{18}O$ increases suggesting a causal link between sequence boundaries traced from the shelf and glacioeustatic changes. Abreu and Haddad (1998) demonstrated a strong stratigraphic relationship between higher frequency shifts in the oxygen isotope record and sequences proposed from the rock record. Therefore, oxygen isotope curves might provide an

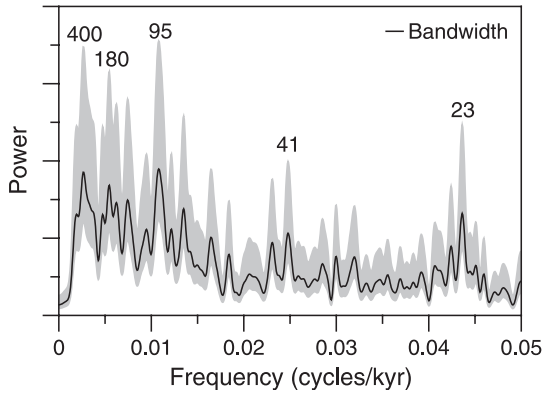

Fig. 8. Blackman–Tukey power spectrum of Site 1085 $\delta^{18}O$ data from 7.3 to 13.8 Ma (black line) with the 80% confidence level (grey area). Strong spectral peaks are present at all orbital frequencies (~400 kyr, ~95 kyr, ~41 kyr, and ~23 kyr). Note the strong peak at ~180 kyr, which might be related to the 174-kyr obliquity cycle. Prior to spectral analysis data were normalized, pre-whitened (enhances power in the high-frequency domain), trend removed, and resampled at 4-kyr intervals.

independent method for stratigraphic calibration of major eustatic changes and demonstrate synchronicity of depositional sequences on different continents. Such links are not unexpected during intervals with large- or even moderate-sized ice-sheets. Evidence for a causal connection between $\delta^{18}O$ increases and sequence boundaries led to the conclusion that variations in the size of ice-sheets have been the primary control on the formation of sequence boundaries since ~42 Ma (Miller et al., 1998). Recently, Billups and Schrag (2002) have shown that major increases in $\delta^{18}O$ of sea-water, calculated from Mg/Ca and $\delta^{18}O$ measurements, are in good agreement with the sequence boundaries of Haq et al. (1987) linking $\delta^{18}O$ increases at Mi-events to sea level regression. Furthermore, Lear et al. (2000) presented evidence that most of the benthic $\delta^{18}O$ increase (~85%) between 15 and 11 Ma can be attributed to an increase in continental ice volume, whereas the

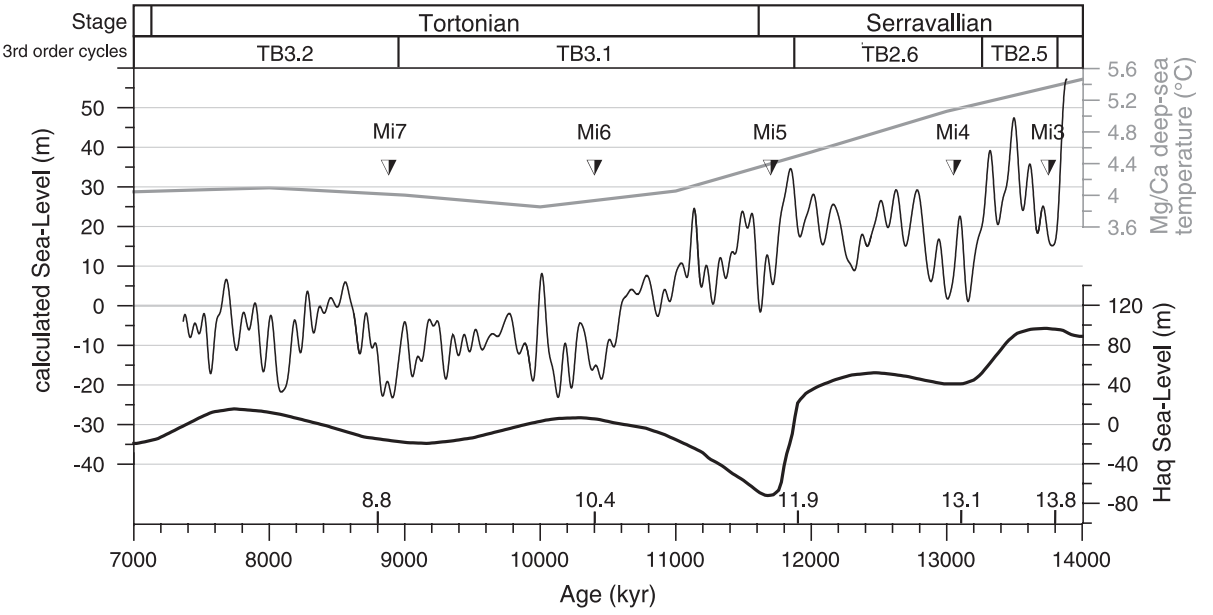

Fig. 9. Comparison of calculated sea-level variations derived from the $\delta^{18}O$ record of Site 1085 (center grey line) and the Haq et al. (1987) sea-level curve (black line). To calculate the middle to late Miocene sea-level variations, we converted the $\delta^{18}O$ carbonate values of Site 1085 into $\delta^{18}O$ seawater values using the simple linear equation of Bemis et al. (1998). The $\delta^{18}O$ seawater values then have been transformed into sea-level variations using the equation of Fairbanks and Matthews (1978) and corrected for deep-sea temperature changes as derived from Lear et al. (2000, top grey line). The 5 age-points at the bottom mark ages of $\delta^{18}O$ inflections published by Miller et al. (1998), which have been interpreted as sequence boundary markers. On top, the sequence boundaries after Haq et al. (1987) and the Stage boundaries after Lourens et al. (2004) are shown.

remaining shift in $\delta^{18}O$ reflects cooling of bottom waters.

At Site 1085, $\delta^{18}O$ increases at Mi-events coincide with enhanced downslope transport of shelf derived terrigenous matter supporting a causal link to sea-level lowstands (Westerhold, 2003) in periods of increased ice-sheet growth on Antarctica. From 13.8 to 10.4 Ma, the overall increase in $\delta^{18}O$ at Site 1085 is 1.1‰. We now assume that 85% of the $\delta^{18}O$ long-term increase is due to ice volume increase (Lear et al., 2000) and that the Pleistocene rate of $\delta^{18}O$/sea-level change is applicable for the Miocene. Using the Pleistocene gradient of 0.11‰ for a 10 m change in sea level (Fairbanks and Matthews, 1978) and the simple linear equation of Bemis et al. (1998) to convert the $\delta^{18}O$ carbonate values into $\delta^{18}O$ seawater values, the increase in benthic $\delta^{18}O$ values resemble sea-level lowering of ~85 m from 13.8 to 10.4 Ma (Fig. 9). This estimate is seemingly unrealistic because it would imply the build up of all modern ice already in the middle to late Miocene. In contrast, if we assume a 3 °C cooling of deep waters as proposed by Billups and Schrag (2002), we end up with only 43 m of sea-level fall. Recent results from the Marion Plateau suggest bottom-water cooling between 1.8 and 2.4 °C and a sea level fall of 50.0±5 m (John et al., 2004) being consistent with the results from the New Jersey Margin (Miller et al., 1998).

The amplitude and timing of the Mi-events (Fig. 9) matches perfectly with the results from Miller et al. (1998) confirming the close relation of sequence boundaries and ice-sheet growth. Comparison to the Haq et al. (1987) sea-level curve suggests close relationship between Mi-events and third-order sea-level variations. For example, the major middle to late Miocene sea-level fall, which has been positioned right before the Serravalian/Tortonian boundary (11.6 Ma after Lourens et al., 2004), is associated with the Mi5 event and the Sequence boundary TB2.6/TB3.1. The major difference between the calculated middle to late Miocene sea-level variations (Fig. 9) to the Haq et al. (1987) curve is the absence of a strong sea-level fall at ~10.5 Ma, prior to the Mi6 event. Miller et al. (1998) also reported that no equivalent sequence boundary can be found in the vicinity of the Mi6 event. If we assume that the 0.3‰ increase in $\delta^{18}O$ values from 10.7 to 10.4 Ma is solely due to a deep-sea temperature decrease, the remaining middle to late Miocene increase in $\delta^{18}O$ represents ~50m of sea-level lowering as proposed by John et al. (2004). The cooling of the deep-sea might be related to the onset of the modern thermohaline circulation between 11 and 10 Ma (e.g. Berger and Wefer, 1996) and attributed major influx of cold waters (AAIW) starting upwelling activity off Namibia (Siesser, 1978; Dieser-Haass et al., 1992). However, future estimates of deep-sea temperatures at Site 1085 have to confirm these findings.

5. Conclusion

The high-resolution benthic stable oxygen isotope data of ODP Site 1085 provide new insight into the middle to late Miocene paleoclimatic evolution. A detailed chronology based on orbitally tuning of a high-resolution Fe intensity composite record has been developed. The long-term cooling trend in $\delta^{18}O$ record of Site 1085 approximates the general trend in the global $\delta^{18}O$ deep-sea composite of Zachos et al. (2001a) resembling the middle to late Miocene buildup of the East Antarctic Ice Sheet. The benthic $\delta^{18}O$ record of Site 1085 shows significant increases with maxima at 13.8, 13.2, 11.7, and 10.4 Ma, corresponding to the Mi-events of Miller et al. (1991). The comparison with other benthic oxygen isotope records shows that the identification of Mi-events is feasible from 13.8 to 10 Ma. Afterwards, the identification is difficult because the amplitude of $\delta^{18}O$ variations is rather small and yields aliasing effects in the lower resolution records. The ages for the Mi-events derived in this study are consistent with the results of Miller et al. (1998) and therefore support a causal link between sequence boundaries traced from the shelf and glacioeustatic changes due to ice-sheet growth.

Spectral analysis of oxygen isotope data document paleoceanographic response to eccentricity and obliquity climate forcing in the middle to late Miocene. The eccentricity-related components in the $\delta^{18}O$ record (400- and 100-kyr) might originate in an asymmetrical response mechanism that preferentially introduces variance from the warmer portion of the eccentricity-modulated precession. A strong spectral peak around 180-kyr might be related to the asymmetry of the obliquity cycle, which also is proposed to

be responsible for the 100-kyr cyclicity (Liu, 1992). Maxima in the $\delta^{18}O$ record, interpreted as glacial periods, correspond to minima in eccentricity and minima in the 174-kyr obliquity modulation. Strong middle to late Miocene glacial events are associated with 400-kyr eccentricity minima and obliquity modulation minima, except Mi4. Therefore, fluctuations in the amplitude of obliquity and eccentricity seem to be the driving force for the middle to late Miocene climate variability.

Acknowledgments

We are indebted to M. Segl and her team for carefully supervising the stable isotope analyses. We thank A. Wuelbers and W Hale for the help at the Bremen Core Repository. This contribution benefits from discussion with C. M. John, K. G. Miller, J. C. Zachos, and L. J. Lourens. T. Kouwenhoven and K. Billups are thanked for their critical review and suggestions for the manuscript. We thank the Ocean Drilling Program for providing samples. This study was funded by the Deutsche Forschungsgemeinschaft (We 992/28) and by the Deutsche Forschungsgemeinschaft as part of the DFG-Research Center 'Ocean Margins' of the University of Bremen No. RCOM0256.

Appendix A. Supplementary data

Supplementary data associated with this article can be found, in the online version, at doi:10.1016/j.palaeo.2004.12.001.

References

Abreu, V.S., Anderson, J.B., 1998. Glacial eustasy during the Cenozoic: sequence stratigraphic implications. AAPG Bull. 82 (7), 1385–1400.

Abreu, V.S., Haddad, G.A., 1998. Glacioeustatic fluctuations: the mechanism linking stable isotope events and sequence stratigraphy from the early Oligocene to middle Miocene. In: De Graciansky, P.-C., Hardenbol, J., Jacquin, T., Vail, P.R., Farley, M.B. (Eds.), Sequence Stratigraphy of European Basins. SEPM Special Publication, Tulsa, pp. 245–259.

Andersson, C., Jansen, E., 2003. A Miocene (8–12 Ma) intermediate water benthic stable isotope record from the northeastern Atlantic, ODP Site 982. Paleoceanography 18 (1).

Backman, J., Raffi, I., 1997. Calibration of Miocene nannofossil events to orbitally tuned cyclostrati-graphies from ceara rise. In: Shackleton, N.J., Curry, W.B., Richter, C., Bralower, T.J. (Eds.), Proc. ODP, Sci. Results, vol. 154. Ocean Drilling Program, College Station, TX, pp. 83–99.

Beaufort, L., 1994. Climatic importance of the modulation of the 100 kyr cycle inferred from 16 m.y. long Miocene records. Paleoceanography 9 (6), 821–834.

Bemis, B.E., Spero, H.J., Bijma, J., Lea, D.W., 1998. Reevaluation of the oxygen isotopic composition of planktonic foraminifera: experimental results and revised paleotemperature equations. Paleoceanography 13 (2), 150–160.

Berger, W.H., Wefer, G., 1996. Expeditions into the past: paleoceanographic studies in the South Atlantik. In: Wefer, G., Berger, W.H., Siedler, G., Webb, D.J. (Eds.), The South Atlantic: Present and Past Circulation. Springer-Verlag, Berlin, pp. 363–410.

Berggren, W.A., Hilgen, F.J., Langereis, C.G., Kent, D.V., Obradovich, J.D., Raffi, I., Raymo, M.E., Shackleton, N.J., 1995a. Late Neogene chronology: new perspectives in high-resolution stratigraphy. Geol. Soc. Amer. Bull. 107, 1272–1287.

Berggren, W.A., Kent, D.V., Swisher III, C.C., Aubury, M.P., 1995b. A revised Cenozoic geochronology and chronostratigraphy. In: Berggren, W.A., Kent, D.V., Aubury, M.P., Hardenbol, J. (Eds.), Geochronology, Time Scales and Global Stratigraphic Correlation, SEPM Spec. Publ., pp. 129–212.

Billups, K., Schrag, D.P., 2002. Paleotemperatures and ice volume of the past 27 Myr revisited with paired Mg/Ca and $^{18}O/^{16}O$ measurements on benthic foraminifera. Paleoceanography 17 (1).

Cande, S.C., Kent, D.V., 1995. Revised calibration of the geomagnetic polarity timescale for the late Cretaceous and Cenozoic. J. Geophys. Res. 100 (B4), 6093–6095.

Christensen, B.A., Maslin, M., 2001. An astronomically calibrated age model for Pliocene site 1085, ODP Leg 175. In: Wefer, G., Berger, W.H., Richter, C., et al. (Eds.), Proc. ODP, Sci. Results, vol. 175, pp. 1–19. [Online]. Available from World Wide Web: <http://www-odp.tamu.edu/publications/175_SR/VOLUME/CHAPTERS/SR175_22.PDF>.

Clemens, S.C., Tiedemann, R., 1997. Eccentricity forcing of Pliocene–Early Pleistocene climate revealed in a marine oxygen-isotope record. Nature 385, 801–804.

Diester-Haass, L., Meyers, P.A., Rothe, P., 1992. The Benguela Current and associated upwelling on the southwest African Margin: a synthesis of the Neogene–Quaternary sedimentary record at DSDP Sites 362 and 532. In: Prell, C.P., Emeis, K.C. (Eds.), Upwelling Systems: Evolution Since the Early Miocene. Geological Society Special Publication, pp. 331–342.

Fairbanks, R.G., Matthews, R.K., 1978. The marine oxygen isotope record in Pleistocene corals, Barbados, West Indies. Quat. Res. 10, 181–196.

Flower, B.P., Kennett, J.P., 1995. Middle Miocene deepwater paleoceanography in the southwest Pacific: relations with East Antarctic Ice Sheet development. Paleoceanography 10 (6), 1095–1112.

Fronval, T., Jansen, E., 1996. Late Neogene paleoclimates and paleoceanography in the Iceland–Norwegian Sea: evidence from the Iceland and Vøring Plateaus. In: Thiede, J., Myhre, A.M., Firth, J.V., Johnson, G.L., Ruddiman, W.F. (Eds.), Proc. ODP, Sci. Results, vol. 151. Ocean Drilling Program, College Station, TX, pp. 455–468.

Hagelberg, T.K., Shackleton, N.J., Pisias, N.G., et al., 1992. Development of Composite Depth Sections for Sites 844 through 854. In: Mayer, L.A., Pisias, N.G., Janecek, T.R., et al. (Eds.), Proc. ODP, Init. Reports, vol. 138. Ocean Drilling Program, College Station, TX, pp. 79–85.

Haq, B.U., Hardenbol, J., Vail, P.R., 1987. Chronology of fluctuating sea levels since the Triassic. Science 235, 1156–1166.

Hilgen, F.J., Krijgsman, W., Raffi, I., Turco, E., Zachariasse, W.J., 2000. Integrated stratigraphy and astronomical calibration of the Serravillian/Tortonian boundary section at Monte Gibliscemi (Sicily Italy). Mar. Micropaleontol. 38, 181–211.

Holbourn, A., Kuhnt, W., Simo, J.A., Li, Q., 2004. Middle Miocene isotope stratigraphy and paleoceanographic evolution of the northwest and southwest Australian margins (Wombat Plateau and Great Australian Bight). Palaeogeogr. Palaeoclimatol. Palaeoecol. 208, 1–22.

Imbrie, J., Berger, A., Boyle, E.A., Clemens, S.C., Duffy, A., Howard, W.R., Kukla, G., Kutzbach, J., Martinson, D.G., McIntyre, A., Mix, A.C., Molfino, B., Morley, J.J., Peterson, L.C., Pisias, N.G., Prell, W.L., Raymo, M.E., Shackleton, N.J., Toggweiler, J.R., 1993. On the structure and origin of major glaciation cycles 2. The 100,000-year cycle. Paleoceanography 8 (6), 699–735.

Jansen, J.H.F., Van der Gaast, S.J., Koster, B., Vaars, A.J., 1998. CORTEX, a shipboard XRF-scanner for element analyses in split sediment cores. Mar. Geol. 151 (1–4), 143–153.

John, C.M., Karner, G.D., Mutti, M., 2004. $\delta^{18}O$ and Marion Plateau backstripping: combining two approaches to constrain late middle Miocene eustatic amplitude. Geology 32 (9), 829–832.

Keller, G., Barron, J.A., 1987. Paleodepth distribution of Neogene deep-sea hiatuses. Paleoceanography 2, 697–713.

Laskar, J., Robutel, P., Joutel, F., Gastineau, M., Correia, A., Levrard, B., 2004. A long-term numerical solution of the insolation quantities of the Earth. Astron. Astrophys. 428, 261–285.

Lear, C.H., Elderfield, H., Wilson, P.A., 2000. Cenozoic deep-sea temperatures and global ice volumes from Mg/Ca in benthic foraminiferal calcite. Science 287, 269–272.

Liu, H.-S., 1992. Frequency variations of the Earth's obliquity and the 100-kyr ice-age cycles. Nature 358, 397–399.

Lourens, L.J., Hilgen, F.J., 1997. Long-periodic variations in the Earth's obliquity and their relation to third-order eustatic cycles and late Neogene glaciations. Quat. Int. 40, 43–52.

Lourens, L.J., Hilgen, F.J., Laskar, J., Shackleton, N.J., Wilson, D., 2004. The Neogene period. In: Gradstein, F., Ogg, J., Smith, A. (Eds.), A geological Timescale.

Miller, K.G., Feigenson, M.D., 1991. Miocene isotope reference section, deep sea drilling project site 608: an evaluation of isotope and biostratigraphic resolution. Paleoceanography 6 (1), 33–52.

Miller, K.G., Wright, J.D., Fairbanks, R.G., 1991. Unlocking the icehouse: Oligocene–Miocene oxygen isotope, eustacy, and margin erosion. J. Geophys. Res. 96, 6829–6848.

Miller, K.G., Mountain, G.S., Browning, J.V., Kominz, M., Sugarman, P.J., Christie-Blick, N., Katz, M.E., 1998. Cenozoic global sea level, sequences, and the New Jersey transect: results from coastal plain and continental slope drilling. Rev. Geophys. 36 (4), 569–601.

Paillard, D., Labeyrie, L., Yiou, P., 1996. Macintosh program performs time-series analysis. Eos Trans. AGU 77 (379) (http://www.agu.org/eos_elec/96097e.html).

Paul, H.A., Zachos, J.C., Flower, B.P., Tripati, A., 2000. Orbitally induced climate and geochemical variability across the Oligocene/Miocene boundary. Paleoceanography 15 (5), 471–485.

Pisias, N.G., Mix, A.C., 1988. Aliasing of the geological record and the search for long-period Milankovitch Cycles. Paleoceanography 3 (5), 613–619.

Röhl, U., Abrams, L.J., 2000. High-resolution, downhole and non-destructive core measurements from sites 999 and 1001 in the Caribbean Sea: application to the late Paleocene thermal maximum. In: Leckie, R.M., Sigurdsson, H., Acton, G.D., Draper, G. (Eds.), Proc. ODP, Sci. Results, vol. 165, pp. 191–203.

Savin, S.M., Douglas, R.G., Stehli, F.G., 1975. Tertiary marine paleotemperatures. Geol. Soc. Amer. Bull. 86, 1499–1510.

Schulz, M., Berger, W.H., Sarnthein, M., Grootes, P.M., 1999. Amplitude variations of 1470-year climate oscillations during the last 100,000 years linked to fluctuations of continental ice mass. Geophys. Res. Lett. 26 (22), 3385–3388.

Shackleton, N.J., Crowhurst, S., 1997. Sediment fluxes based on an orbitally tuned time scale 5 to 14 Ma, site 926. In: Shackleton, N.J., Curry, W.B., Richter, C., Bralower, T.J. (Eds.), Proc. ODP, Sci. Results, vol. 154. Ocean Drilling Program, College Station, TX, pp. 69–82.

Shackleton, N.J., Hall, M.A., 1997. The late Miocene stable isotope record, site 926. In: Shackleton, N.J., Curry, W.B., Richter, C., Bralower, T.J. (Eds.), Proc. ODP, Sci. Results, vol. 154. Ocean Drilling Program, College Station, TX, pp. 367–373.

Shackleton, N.J., Kennett, J.P., 1975. Paleotemperature history of the Cenozoic and the initiation of Antarctic glaciation: oxygen and carbon isotope analyses in DSDP sites 277, 279, and 281. In: Kennett, J.P., Houtz, R.E., et al. (Eds.), Init. Repts. DSDP, vol. 29. U.S. Govt. Printing Office, Washington, pp. 743–755.

Shackleton, N.J., Crowhurst, S.J., Weedon, G.P., Laskar, J., 1999. Astronomical calibration of Oligocene–Miocene time. In: Shackleton, N.J., McCave, I.N., Weedon, G.P. (Eds.), Phil. Trans. R. Soc. Lond. A., pp. 1907–1929.

Short, D.A., Mengel, J.G., Crowley, T.J., Hyde, W.T., North, G.R., 1991. Filtering of Milankovitch cycles by earth's geography. Quat. Res. 35, 157–173.

Siesser, W.G., 1978. Aridification of the Namib Desert: evidence from oceanic cores. In: Zinderen-Bakker, V. (Ed.), Antarctic Glacial History and World Paleoenvironment. Balkema, Rotterdam, pp. 105–112.

Turco, E., Hilgen, F.J., Lourens, L.J., Shackleton, N.J., Zachariasse, W.J., 2001. Punctuated evolution of global climate cooling during the late Middle to early Late Miocene: high-resolution

planktonic foraminiferal and oxygen isotope records from the Mediterranean. Paleoceanography 16 (4), 405–423.

Turco, E., Bambini, A.M., Foresi, L., Iaccarino, S., Lirer, F., Mazzei, R., Salvatorini, G., 2002. Middle Miocene high-resolution calcareous plankton biostratigraphy at Site 926 (Leg 154, equatorial Atlantic Ocean): palaeoecological and palaeobiological implications. Geobios 35, 257–276 (Mémoire spécial no. 24).

Vidal, L., Bickert, T., Wefer, G., Röhl, U., 2002. Late Miocene stable isotope stratigraphy of Site 1085: relation to Messinian events. Mar. Geol. 180, 71–85.

Vincent, E., Berger, W.H., 1985. Carbon dioxide and polar cooling in the Miocene: the Monterey hypothesis. In: Sundquist, E.T., Broecker, W.S. (Eds.), The carbon cycle and atmospheric CO_2: natural variations Archean to present. AGU, Washington, DC, pp. 455–468.

Wefer, G., Berger, W.H., Richter, C., et al., 1998. Proc. ODP, Init. Repts., vol. 175. Ocean Drilling Program, College Station, TX. 385–428 pp.

Westerhold, T., 2003. The Middle Miocene Carbonate Crash: Relationship to Neogene Changes in Ocean Circulation and Global Climate. Dissertation thesis, Bremen, Bremen. 137 pp.

Westerhold, T., Bickert, T., Vidal, L., submitted for publication. Pleistocene Oxygen Isotope Stratigraphy of ODP Site 1085-SE Atlantic. Earth Planet. Sci. Lett.

Wright, J.D., Miller, K.G., 1992. Miocene stable isotope stratigraphy, site 747, Kerguelen Plateau. In: Wise Jr., S.W., Schlich, R., et al., (Eds.), Proc. ODP, Sci. Results, vol. 120. Ocean Drilling Program, College Station, TX, pp. 855–866.

Wright, J.D., Miller, K.G., Fairbanks, R.G., 1992. Early and middle Miocene stable isotopes: implications for deepwater circulation and climate. Paleoceanography 7 (3), 357–389.

Zachos, J.C., Flower, B.P., Paul, H., 1997. Orbitally paced climate oscillations across the Oligocene/Miocene boundary. Nature 388, 567–570.

Zachos, J., Pagani, M., Sloan, L., Thomas, E., Billups, K., 2001a. Trends, rhythms, and aberrations in global climate 65 Ma to present. Science 292, 686–693.

Zachos, J., Shackleton, N.J., Revenaugh, J.S., Pälike, H., Flower, B.P., 2001b. Climate response to orbital forcing across the Oligocene–Miocene boundary. Science 292, 274–278.